

Predominance diagrams of uranium and plutonium species in both lithium chloride–potassium chloride eutectic and calcium chloride

L. D. Brown · R. Abdulaziz · S. Simons ·
D. Inman · D. J. L. Brett · P. R. Shearing

Received: 14 May 2013 / Accepted: 8 August 2013 / Published online: 28 August 2013
© The Author(s) 2013. This article is published with open access at Springerlink.com

Abstract Electro-reduction of spent nuclear fuel has the potential to significantly reduce the amount of high level waste from nuclear reactors. Typically, spent uranium and plutonium are recovered via the PUREX process leading to a weapons-grade recovery; however, electro-reduction would allow spent nuclear fuel to be recovered effectively whilst maintaining proliferation resistance. Here, we present predominance diagrams (also known as Littlewood diagrams) for both uranium and plutonium species in molten lithium chloride–potassium chloride eutectic (LKE) at 500 °C and in calcium chloride at 800 °C. All diagrams presented depict regions of stability of various phases at unit activity in equilibrium with their respective dissociated ions. The diagrams thermodynamically define the electrochemical system leading to predictions of reaction conditions necessary to electrochemically separate species. The diagrams have been constructed using a pure thermodynamic route; identifying stable species within the molten salt with an assumption of unit activity for each of the phases. These thermodynamically predicted diagrams have been compared to the limited available experimental data; demonstrating good correlation. The diagrams can also be used to predict regions of stability at activities less than unity and is also demonstrated.

Keywords Nuclear material · Molten salts · E-pO²⁻ · Electrochemical reduction · Predominance diagrams · Littlewood diagrams

L. D. Brown · R. Abdulaziz · S. Simons · D. Inman ·
D. J. L. Brett · P. R. Shearing (✉)
Electrochemical Innovation Laboratory, Department of
Chemical Engineering, University College London, Torrington
Place, London WC1E 7JE, UK
e-mail: p.shearing@ucl.ac.uk

1 Introduction

In the UK, nuclear fission will play a significant role in near and medium term decarbonisation of electricity supply; however, concerns regarding nuclear reactor safety, nuclear waste reprocessing and disposal and nuclear fuel proliferation remain significant barriers to widespread acceptance of this technology.

Whilst nuclear reactor safety is being significantly improved with generation III+ reactors, such as the European pressurised reactor (EPR) which demonstrates improved tolerance to earthquakes and aircraft crashes, there remains concern regarding nuclear waste, which has, unfortunately, not received the same degree of recent progress. Electro-reduction of metal oxides to their metallic phases has become increasingly popular since the FFC Cambridge process was realised and elucidated in the first decade of the twenty first century [1–5]. This process allows the reduction of metal oxides to its respective metallic form in an electrochemical cell using a molten chloride electrolyte. To date, the application of the FFC Cambridge process has been primarily concerned with the electro-reduction of TiO₂ using a molten CaCl₂ melt. One possible application of the FFC Cambridge process in the nuclear re-processing industry is the electro-reduction of uranium oxides, plutonium oxides, and other rare earth metals and actinides to their respective metallic phases in a molten salt environment. Research activities in the USA and Asia have demonstrated the separation of actinides and rare earth metals using electrochemical processes such as electro-refining and electrolysis [6, 7].

In molten salt reaction media, the electrolysis potentials are a function of the negative logarithm of the activity of O²⁻ ions in the melt (pO²⁻). This oxo-base phenomenon is analogous to pH in Pourbaix diagrams where the O²⁻ ions

play the same role as H^+ ions in aqueous oxo-acidity media. These types of diagrams were first published by Littlewood [8] in 1962 and are therefore also referred to as Littlewood diagrams.

Experimentally determined Littlewood diagrams for uranium [9–12] and plutonium species [13–15] in molten lithium chloride–potassium chloride eutectic (LKE) exist in the literature; however, there are no such diagrams presented for both of these species in calcium chloride. Moreover, with the exception of the work done by Caravaca et al. [15], the diagrams presented were calculated in the absence of the extensive thermodynamic data now available. The previously presented diagrams depict regions of stability for the phases using anodic titration methods and as such at least one of the species has activity of less than unity.

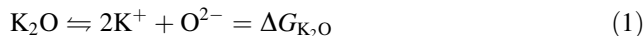
This paper presents a theoretical prediction of stable phases in the two molten salt melts, where the regions of stability are separated by the conditions necessary for both species to co-exist in the melt both at unit activity. We also demonstrate how one would deduce the diagrams, thermodynamically, if one or more of the species is present at an activity less than unity.

Littlewood diagrams are valuable tools for prediction of the conditions required for direct reduction (DR) to selectively reduce actinides to their metallic phases. Moreover, the diagrams for different systems can be superimposed to deduce the feasibility of selective DR. The work presented here is an investigation into the behaviour of both uranium and plutonium species in molten LKE at 500 °C and in $CaCl_2$ at 800 °C and focusses on the inherent conditions required to selectively reduce both species using DR.

2 Methodology and calculations

In order to describe the system, we must define the zero standard cell potential as the standard potential of the chlorine electrode in contact with a chloride fused salt melt at unit chloride activity [8]. It is also important to note that the use of this convention forces the free energy of dissociation of chlorine to zero Joules. As the system contains oxide ions, rather than H^+ ions, it is necessary to define the free energy change of the oxide ion. Convention dictates this to be defined as the pure oxide of the cation of the chloride melt as unit activity of the oxide ion. Here, we examine a eutectic mixture. Therefore, the oxide ions, which are a minority in the melt, will have a lithium ion–potassium ion–chloride ion environment as their nearest neighbour shells. These chloride ions are produced by both metal chlorides in the melt and so a molar average of the eutectic is used to calculate the free energy of oxide ions. All of the thermodynamic data used in the calculations is shown in Table 1.

In a pure potassium chloride melt, the standard state of oxide ions would be K_2O . The reaction to form oxide ions would thus be



The standard free energy of formation of the oxide ion in potassium chloride can therefore be defined as

$$\Delta G^\circ O_2(K) = \Delta G_{K_2O}^\circ - 2\Delta G^\circ K \quad (2)$$

where $\Delta G^\circ K$ is equal to $\Delta G^\circ KCl$

Similarly, Eqs. 2 and 3 can be written for Li_2O :



$$\Delta G^\circ O_2(Li) = \Delta G_{Li_2O}^\circ - 2\Delta G^\circ Li \quad (4)$$

Leading to the free energy of oxide ion in the eutectic to be:

$$\Delta G^\circ O_2 = 0.41\Delta G^\circ O_2(Li) + 0.59\Delta G^\circ O_2(K) \quad (5)$$

In order to derive Eq. 5, it is assumed that the eutectic is an ideal mixture: The enthalpy of mixing is zero. It is also assumed that the system is isothermal with a constant vapour pressure. Table 1 contains all of the thermodynamic data used here. At 500 °C, the standard free energy of K_2O and KCl are -252.77 and -362.66 kJ mol^{-1} , respectively. For Li_2O and $LiCl$, the values are -496.75 and -344.85 kJ mol^{-1} , respectively. By taking a weighted average of oxide ions produced from lithium and potassium, a standard free energy of oxide ions in the melt is calculated to be -357.91 kJ mol^{-1} .

The Gibbs free energy of formation of a compound is related to the standard cell reduction potential via the following equation

$$E^\circ = \frac{-\Delta G^\circ}{nF} \quad (6)$$

The potential required for reduction and the pO^{2-} are related via the Nernst equation:

$$E = E^\circ - \frac{RT}{nF} \ln(Q) \quad (7)$$

where Q is the reaction quotient and parentheses denote activities. The lines separating two phases define the conditions where both species co-exist within the melt and therefore both have activities of unity. This phenomenon allows for Equation 6 to be written in a more suitable form:

$$E = E^\circ - \frac{2.303RT}{nF} \log(O^{2-}) \quad (8)$$

Equation 7 is used for the three different types of reaction that can occur in a molten salts system. The first is where the reaction is a function of both electron transfer and oxide ion activity which defines the diagonal lines on the Littlewood diagrams, leading to use of Eq. 8; secondly,

Table 1 Free energy change for nuclear materials at 500 and 800 °C

Species	ΔG_f° (kJ mol ⁻¹) at 500 °C	ΔG_f° (kJ mol ⁻¹) at 800 °C	References
Li ₂ UO ₄ (CaUO ₄ at 800 °C)	-1,662.68 ^a	(-1,621.46)	[16, 17]
UO ₂	-950.56	-898.31	[18, 19]
U ₄ O ₉	-3,921.20	-3,696.25	[19, 20]
U ₃ O ₈	-3,055.66	-2,861.05	[19, 21]
UO ₃	-1,023.70	-984.84	[19, 22, 23]
UCl ₂ O	-882.87	-825.83	[17, 21]
U ₂ Cl ₅ O ₂	-1,796.82	-1,651.52	[24]
UCl ₃	-693.80	-631.16	[17, 24]
UCl ₄	-794.60	-723.98	[22, 25]
PuO ₂	-908.53	-851.971184	[21, 23]
Pu ₂ O ₃	-1,475.28	-1,396.98	[22, 23]
PuOCl	-814.03	-757.88	[17, 18]
PuCl ₃	-786.59	-725.12	[17]
LiCl (CaCl ₂ at 800 °C)	-344.85	(-522.22)	[22, 26, 27]
Li ₂ O (CaO at 800 °C)	-496.75	(-634.73)	[19, 22, 23]
KCl	-362.66		[20, 28]
K ₂ O	-252.77		[19, 23]

^a Extrapolated above 300 K

reactions that are independent of oxide ion activity, give rise to horizontal lines and in this case, Eq. 8 can be re-written as:

$$pO^{2-} = \frac{\Delta G^o}{2.303RT} \tag{9}$$

Finally reactions that are independent of oxide ions, correspond to the vertical lines of the Littlewood diagrams, for these reactions Eq. 8 may be re-written as:

$$E = E^o = \frac{-\Delta G^o}{nF} \tag{10}$$

The relationship between the oxygen pressure, potential, and oxide activity via the Nernst equation is given by:

$$E = E^o + \frac{2.303RT}{nF} \log \left(\frac{(O_2)^{0.5}}{O^{2-}} \right) \tag{11}$$

3 Results and discussion

Using the methodology outlined above, Littlewood diagrams have been created for both uranium species and plutonium species in LKE at 500 °C and in CaCl₂ at 800 °C. The uranium species are presented in Fig. 1 and the plutonium species are presented in Fig. 2.

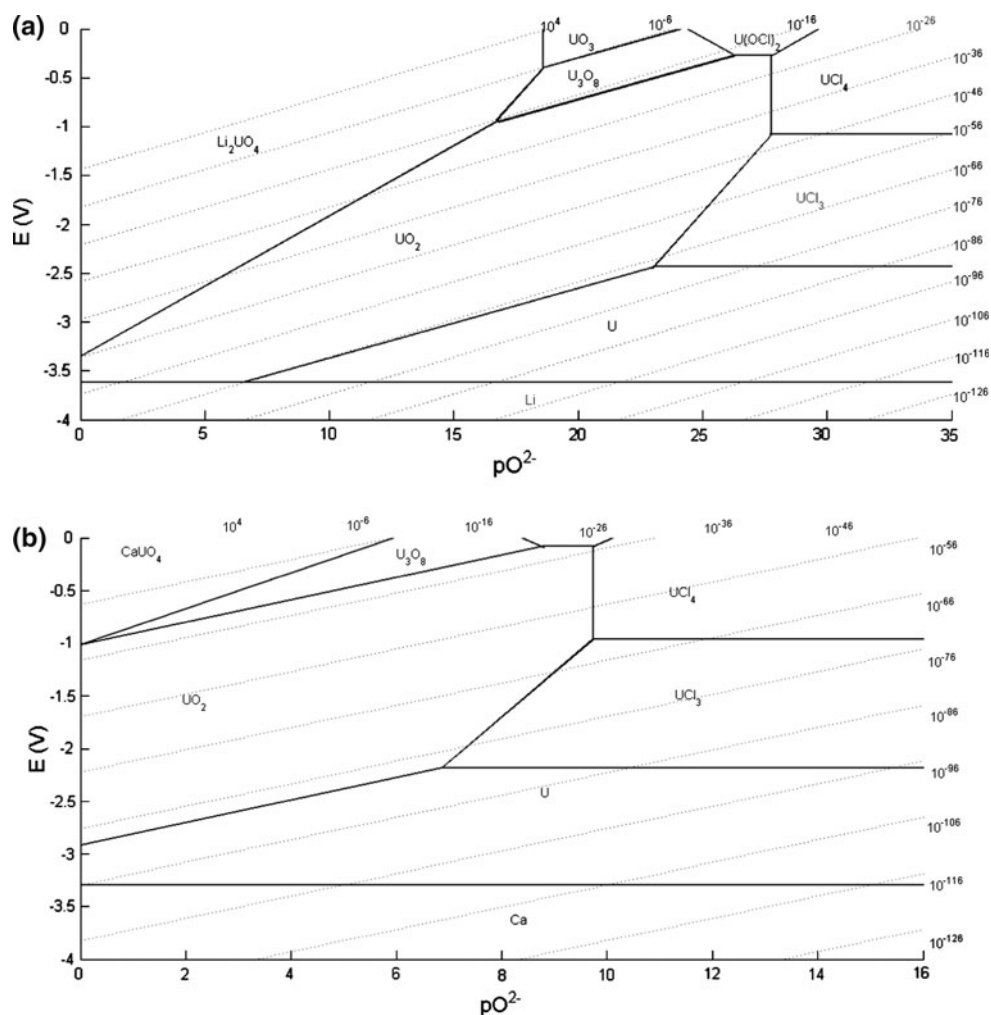
3.1 Uranium Littlewood diagrams

Figure 1 shows the Littlewood diagram for uranium species in (a) LKE and (b) CaCl₂. The diagonal dotted lines show the relationship between potential, oxygen pressure and oxide activity. Oxygen pressures in excess of 10⁴

would see the oxygen exist with an atmospheric pressure. The lines show oxygen pressures down to extremely low values which are particularly useful in systems containing metals as they have a high affinity towards oxygen. For example, if an electrochemical cell was prepared in an atmosphere of argon containing 1 ppm by volume of water vapour, this vapour would be in equilibrium with an oxygen partial pressure of 10⁻⁴⁰. One could then deduce the activity of oxygen that would exist in equilibrium with oxygen. This could be useful to deduce what conditions were/are present in electrochemical cells. The solid black lines depict regions of stability of adjacent phases that would both coexist with unit activity. Perhaps the most striking comparison of the diagrams (Fig. 1) is differences in location of the phases; in the calcium chloride melt the region of stability for UO₂ is smaller and is shifted to lower pO²⁻ values by comparison with LKE. This is explained thermodynamically; as the temperature of the system is increased, the Gibbs free energy change of the electrochemical reaction is less negative and, therefore, the Nernst potential becomes less negative for given activities of oxide ions.

It is also important to note that the electro-reduction of UO₂ to metallic U in LKE is more facile at higher temperatures, with respect to controlling the pO²⁻ of the melt. This is due to the fact that at low temperatures and low values of pO²⁻ (ca. 0–6) lithium deposition would occur preferentially to the oxide reduction. In this case, it would be necessary to control the pO²⁻ within the melt sufficiently to be able to reduce UO₂ to U at unit activity. Conversely, one could also ensure the activity of UO₂ in

Fig. 1 Uranium species in **a** LKE at 500 °C and **b** CaCl₂ at 800 °C



the melt is low enough to allow this electrochemical reaction to occur at lower values of pO^{2-} , which is described later in this paper.

3.2 Plutonium Littlewood diagrams

Figure depicts the plutonium species in LKE (a) and CaCl₂ (b). Again, comparison of CaCl₂ with LKE shows the regions for stability of the plutonium species is shifted to lower pO^{2-} .

As spent reactor products may be expected to contain both uranium and plutonium compounds (alongside other rare earths and actinides), it is desirable to thermodynamically predict the feasibility of selective electro-reduction and separation of these species; this can be achieved by super-imposition of the Pu- and U-based diagrams in LKE, as shown in Fig. 3. It can, therefore, be seen that there would be an inherent difficulty at separating both species at unit activity due to the reduction potentials of UO₂|U and Pu₂O₃|Pu being very similar. However, the reduction

potentials of PuOCl|Pu, and UO₂|U diverge at higher pO^{2-} values, leading to a greater possibility of being able to selectively reduce to metallic species.

Figure 3 provides a priori guidelines to inform the experimental conditions required for selective reduction of mixed oxides; for example, if metallic uranium is desired by reducing a mixture of uranium and plutonium, one would be able to achieve this as the reduction potential of UO₂|U is more positive than that of the Pu₂O₃|Pu reduction potential. The lines are, however, very close to one another and give a narrow region whereby reduction to produce metallic uranium only, as depicted by point A in Fig. 3. One could increase the region of stability of metallic uranium by manipulating conditions within the cell. For example, by increasing the pO^{2-} to a value higher than 11 one could work in region B, which has a greater region of stability of uranium. This shows that the diagrams are very useful for predicting the reaction conditions necessary to produce the required product.

Fig. 2 Plutonium species in **a** LKE at 500 °C and **b** CaCl₂ at 800 °C

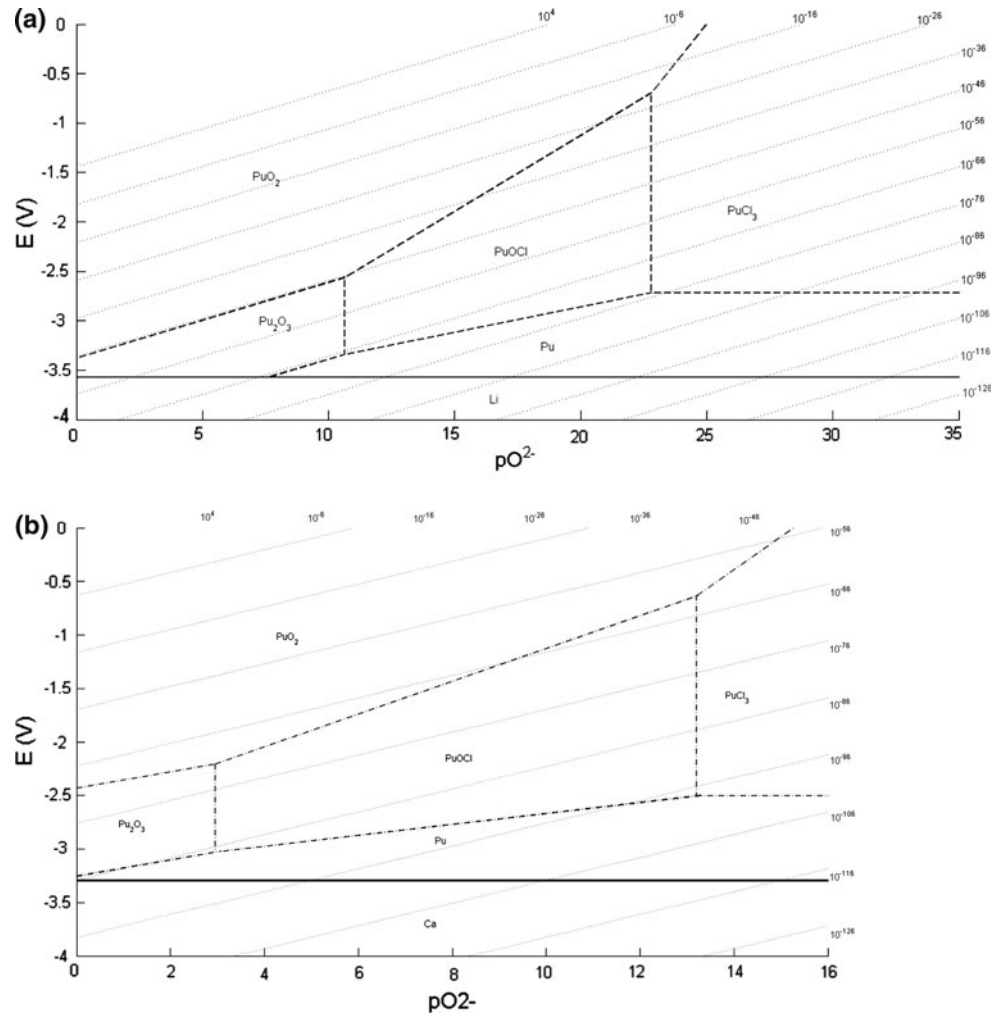


Fig. 3 Uranium and plutonium species in LKE at 500 °C. **a** Shows a narrow window for selective reduction to metallic uranium only at low pO_2^- values. **b** Shows a larger region of stability for metallic uranium at higher values of pO_2^-

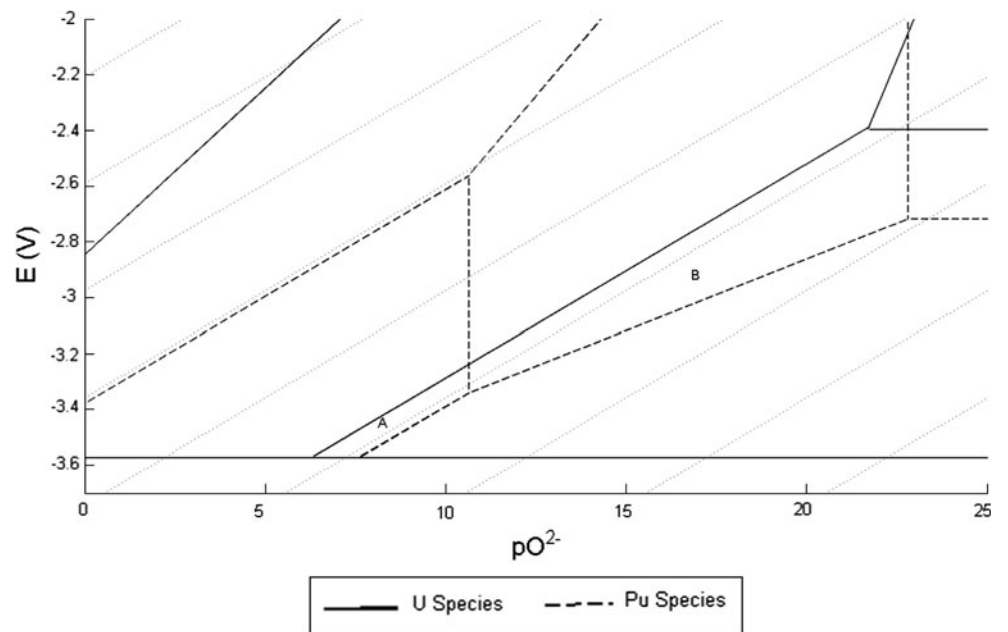
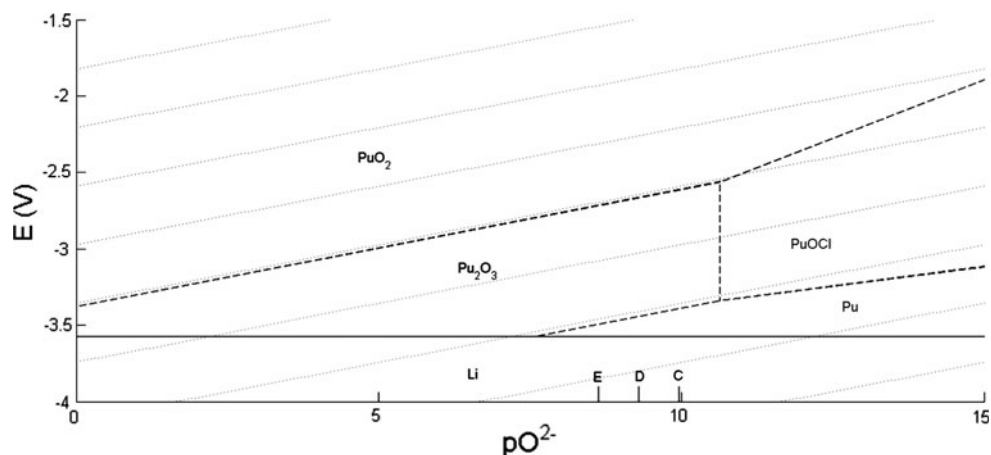


Fig. 4 Plutonium species in LKE at 500 °C with varying PuOCl activity



3.3 Differences between previously published diagrams

In previously published papers containing Littlewood diagrams of uranium and plutonium, information has been empirically derived through titration methods of the nuclear elements into the molten salt. It is important to note that the activities of these nuclear species are all less than unity (approximately, in concentrations of 0.02 mol kg^{-1}) [15] and therefore the location of lines depicting regions of stability are shifted to different $p\text{O}^{2-}$ values.

The theoretical approach adopted here is inherently more flexible in accounting for the effects of changing activity: as an example, if one were to take the concentration of PuOCl to be $1 \times 10^{-2} \text{ mol kg}^{-1}$ (an approximation to the activity) then the $p\text{O}^{2-}$ value at the equilibrium of $\text{Pu}_2\text{O}_3|\text{PuOCl}$ would be shifted left on the diagrams to lower $p\text{O}^{2-}$, this can be calculated as follows:

$$E^0 = \frac{2.303RT}{nF} \log \left(\frac{[\text{Pu}_2\text{O}_3]}{([\text{PuOCl}]^2)([\text{O}^{2-}]^3)} \right) \quad (12)$$

In this example, we consider the activity of Pu_2O_3 to be unity and simplify the Equation 12 to:

$$p\text{O}^{2-} = \frac{\Delta G}{3 \times 2.303RT} + \frac{2}{3} \log(\text{PuOCl}) \quad (13)$$

In Fig. 4, points C, D, and E show where the line would be if the activity of PuOCl was 10^{-1} , 10^{-2} , and 10^{-3} , respectively. It can therefore be seen that one would be able to alter these regions by changing the activity of the appropriate species within the melt. Lower activities could be used, for example, creating larger regions of stability. This, in turn, would allow one to increase region A in Fig. 3. It should also be noted that these lines would also differ slightly is the concentration (or activity) if two adjacent species were less than unity and can be calculated using the same methodology.

4 Conclusion

Littlewood diagrams are a valuable tool for predicting experimental conditions for electro-reduction of spent nuclear fuel. For the first time known to the authors, diagrams for uranium and plutonium species in LKE have been presented via a calculation based on thermodynamic values taken from the literature. Inherently, these diagrams are limited by the thermodynamic data available but they provide a useful tool to predict the state of molten salt systems.

Although the eutectic is assumed to be ideal, the diagrams agree with previously published diagrams obtained experimentally, allowing for changes in species activity. Moreover, there is no issue of complex ion formation in the LKE mixture and so ideality is a good approximation to real system. The diagrams presented allow for the thermodynamic prediction of separation of these species via a direct electrochemical reduction technique.

The electrochemical reduction of UO_2 to metallic uranium is more facile at higher temperatures, as at lower temperatures there is a need to control the $p\text{O}^{2-}$ values to ensure electrochemical decomposition of the melt is not favoured over the electrochemical reduction process. Moreover, superimposition of the uranium and plutonium Littlewood diagrams in LKE show a narrow window for selective reduction to metallic uranium in a mixed oxide system containing both UO_2 and PuO_2 .

Lastly, the authors have shown techniques that can be used in molten salt electrochemical cell design to be able to selectively favour electrochemical reactions.

Acknowledgments This work was carried out as part of the UK Engineering and Physical Sciences Research Council (EPSRC) funded REFINE consortium (<http://www.refine.eng.ed.ac.uk/>). We gratefully acknowledge this EPSRC financial support (EP/J000531/1). PS acknowledges financial support from the Royal Academy of Engineering.

Open Access This article is distributed under the terms of the Creative Commons Attribution License which permits any use, distribution, and reproduction in any medium, provided the original author(s) and the source are credited.

References

1. Chen GZ, Fray DJ, Farthing TW (2000) Direct electrochemical reduction of titanium dioxide to titanium in molten calcium chloride. *Nature* 407(6802):361–364. doi:10.1038/35030069
2. Dring K, Dashwood R, Inman D (2005) Voltammetry of titanium dioxide in molten calcium chloride at 900 °C. *J Electrochem Soc* 152(3):E104–E113
3. Schwandt C, Fray DJ (2005) Determination of the kinetic pathway in the electrochemical reduction of titanium dioxide in molten calcium chloride. *Electrochim Acta* 51(1):66–76. doi:10.1016/j.electacta.2005.03.048
4. Alexander DTL, Schwandt C, Fray DJ (2006) Microstructural kinetics of phase transformations during electrochemical reduction of titanium dioxide in molten calcium chloride. *Acta Mater* 54(11):2933–2944. doi:10.1016/j.actamat.2006.02.049
5. Bhagat R, Dye D, Raghunathan SL, Talling RJ, Inman D, Jackson BK, Rao KK, Dashwood RJ (2010) In situ synchrotron diffraction of the electrochemical reduction pathway of TiO₂. *Acta Mater* 58(15):5057–5062. doi:10.1016/j.actamat.2010.05.041
6. Laidler JJ (1993) Development of IFR pyroprocessing technology. In: Proceedings of global 1993 conference—future nuclear systems: emerging fuel cycles and disposal options
7. Laidler JJ (1993) Pyrochemical recovery of actinides. *Proc Am Power Conf* 55(2):1074–1078
8. Littlewood R (1962) Diagrammatic representation of the thermodynamics of metal-fused chloride systems. *J Electrochem Soc* 109(6):525
9. Molina R (1961) Propriétés chimiques de quelques composés de l'uranium dans les chlorures alcalins fondus. *Bull Soc Chim Fr* 6:1184–1190
10. Landresse G, Duyckaerts G (1973) Diagramme potential/pO²⁻ de l'uranium dans l'eutectique LiCl–KCl fondu. *Anal Chim Acta* 65(1):245–247
11. Uchida I, Niikura J, Toshima S (1981) Electrochemical study of Uo22+–Uo2+–Uo2 system in molten LiCl+KCl eutectic. *J Electroanal Chem* 124(1–2):165–177. doi:10.1016/0368-1874(81)87115-8
12. Martinot L, Fuger J (1986) Determination of solubility products of various actinide oxides in the (Na–K)Cl and (Li–K)Cl eutectics and calculation of new potential-pO²⁻ diagrams. *J Less-Common Met* 120(2):255–266. doi:10.1016/0022-5088(86)90650-8
13. Martinot L, Duyckaerts G (1973) Diagrammes potentiel/pO²⁻ du neptunium et du plutonium dans l'eutectique LiCl–KCl. *Anal Chim Acta* 66(3):474–476
14. Landresse G, Duyckaerts G (1974) Étude par spectrophotométrie d'absorption des propriétés chimiques du plutonium dans l'eutectique LiCl–KCl fondu. *Anal Chim Acta* 73(1):121–127
15. Caravaca C, Laplace A, Vermeulen J, Lacquement J (2008) Determination of the E-pO²⁻ stability diagram of plutonium in the molten LiCl–KCl eutectic at 450°C. *J Nucl Mater* 377(2):340–347
16. Binnewies M, Milke E (2002) Thermochemical data of elements and compounds. Wiley, Weinheim
17. NEA, Guillaumont R, Mompean FJ (2003) Update on the chemical thermodynamics of uranium, neptunium, plutonium, americium and technetium. Elsevier, Amsterdam
18. Barin I (1977) Thermodynamical data of pure substances. VCH Verlags Gesellschaft, Weinheim
19. Landolt-Bornstein (2001) Thermodynamic properties of inorganic materials. Springer, Berlin
20. Barin I (1995) Thermodynamical data of pure substances. VCH Verlags Gesellschaft, Weinheim
21. Barin I (1989) Thermodynamical data of pure substances. VCH Verlags Gesellschaft, Weinheim
22. Barin I (1993) Thermodynamical data of pure substances. VCH Verlags Gesellschaft, Weinheim
23. Glushko V (1994) Thermocenter of the Russian Academy of Sciences. IVTAN Association. *Izhorskaya* 13(19):127412
24. Knacke O, Kubaschewski O, Hesselmann K (1991) Thermodynamic properties of inorganic substances. Springer, Düsseldorf
25. Landolt-Bornstein (2000) Thermodynamic properties of inorganic materials. Springer, Berlin
26. Chase MW (1998) NIST-JANAF thermochemical tables. American Institute of Physics, New York
27. Landolt-Bornstein (1999) Thermodynamic properties of inorganic materials. Springer, Berlin
28. Archera DG (1999) Thermodynamic Properties of the KCl+H₂O System. *J Phys Chem Ref Data* 28(1)